

Effects of species concentration and external resistance on spatiotemporal dynamics during the electro-oxidation of sulfide ion on a platinum disk electrode

Jiaping Yang · You Jia · Qingyu Gao · Changwei Pan ·
Yuemin Zhao · Wenyang Bi · Guangyuan Xie

Received: 9 July 2014 / Revised: 14 February 2015 / Accepted: 17 February 2015
© Springer-Verlag Berlin Heidelberg 2015

Abstract Sulfide and hydroxide ions, acting as negative and positive feedback species of the oscillatory electro-oxidation of sulfide on a platinum disk, respectively, strongly affected the spatiotemporal dynamics of the process. Oscillations with both hidden N-shaped and N-shaped negative differential resistances were enhanced in both amplitude and potential range with increasing sulfide ion concentration, but weakened with increasing hydroxide ion concentration. The patterns in the N-shaped negative differential resistance oscillatory region changed from local pulses to global synchronous oscillations of sulfur deposition and dissolution with increasing sulfide ion concentration. However, as the hydroxide ion concentration increased, both the patterns and oscillations were suppressed and the pulse width also decreased. External resistance was another factor that caused complex oscillations and a novel pattern formation that was observed to be alternating between local pulses and synchronous oscillations of sulfur deposition and dissolution. A detailed analysis of the reaction mechanism and a model simulation provided a reasonable explanation of these phenomena and the dynamic features. This investigation further promoted analysis of the complex spatiotemporal dynamics of the sulfide electro-oxidation system and enriched the experimental results available in electrochemical systems. This research was helpful in the prediction and control of pattern formation processing through adjustment of the positive and negative feedbacks as well as spatial couplings.

Electronic supplementary material The online version of this article (doi:10.1007/s10008-015-2799-6) contains supplementary material, which is available to authorized users.

J. Yang · Y. Jia · Q. Gao (✉) · C. Pan · Y. Zhao · W. Bi · G. Xie (✉)
College of Chemical Engineering, China University of Mining and Technology, Xuzhou 221008, China
e-mail: gaoqy@cumt.edu.cn
e-mail: xgywl@cumt.edu.cn

Keywords Sulfide electro-oxidation · Oscillation · Self-organized pattern · Concentration effect · External resistance

Introduction

Spatiotemporal dynamical phenomena such as multiple states, oscillations, and self-organized patterns have been widely investigated for various electrochemical systems, e.g., metal dissolution [1, 2] and deposition [3, 4], fuel cells [5], and complex electrochemical networks [6]. The electrochemical instabilities are most frequently involved in the occurrence of a negative differential resistance (NDR) [7–10] in the current–potential characteristics. The most common type of NDR is the N-shaped NDR (N-NDR), which is associated with an N-shaped current–potential curve. In the N-NDR system, the electrode potential acts as the positive feedback variable while the mass-transfer limited process provides the general negative feedback. Otherwise, in an N-NDR system with strongly adsorbing ions [11, 12] or with an appropriate external resistance in series in the circuit [13], the NDR could be hidden and oscillations would occur in the positive slope branch of current–potential curve; this is classified as hidden N-shaped NDR (HN-NDR) oscillation. It was previously found that the cell geometry and the external resistor could both affect the spatial coupling of this type of electrochemical system [14–16]. The electrochemical patterns originate from the interplay between the homogeneous dynamics and the spatial coupling. Therefore, by adjusting the various positive (or negative) feedbacks and the different spatial couplings (e.g., local, nonlocal and global coupling) [8, 17–20], the electrochemical system could display complex spatiotemporal dynamic behaviors.

Sulfides are widely distributed in fossil fuels, metal ores, and waste water, which results in environmental pressures during the use and emission of these materials. Therefore, this has stimulated research interest in the dynamics and control of sulfide (electro) oxidation for the development of desulfurization technology. In terms of dynamic instabilities during the electrochemical oxidation of sulfides, Helms et al. [21] first reported both potential and current oscillations during the electrochemical oxidation of sulfides on platinum. Later, Feng et al. [22] and Chen et al. [23] extended the study of the dynamic phenomena and mechanistic features of the electrochemical oxidation process. Multiple oscillatory regions showing N-NDR and HN-NDR characteristics were observed in the current–potential curve, and rich spatiotemporal patterns were formed on the platinum electrode surfaces [13]. When perturbed with chloride ions, which in turn give rise to another NDR [24], the sulfide electrochemical system showed intensive HN-NDR oscillations and the pattern structures were altered, including switching from pulses to uniform oscillations and reduced pulse widths with increasing $[Cl^-]$ content.

Because the hydroxide ion and the sulfide ion act as the positive and negative feedback species, respectively, a systematic study of the effects of these species on the spatiotemporal dynamics is required for model construction and analysis. In addition, possible interactions between the N-NDR and HN-NDR oscillations would produce complex oscillations and result in new spatiotemporal patterns through adjustment of the external resistance. Therefore, in this work, we investigate the effects of both the sulfide and hydroxide ion concentrations and the external resistance on the spatiotemporal dynamics during the electro-oxidation of sulfide on a platinum disk to enable control of the spatiotemporal dynamics in electrochemistry.

Experimental section

A conventional three-electrode cell was used in all experiments. The working electrode (WE) was a platinum disk (2.0 mm in diameter) that was embedded in a Teflon insulator. A 0.5-mm platinum wire that was formed into a ring with diameter of 4.0 cm was used as the counter electrode (CE), and was arranged below the WE at a distance of 1.5 cm. A J-shaped reversible hydrogen electrode (RHE) filled with 0.50 mol L⁻¹ sulfuric acid served as the reference electrode (RE); its tip was close to the WE surface, at a distance of 1.0 mm, and all potentials measured in the experiments were quoted with reference to the RHE. All experiments were conducted on a CHI-660A electrochemical workstation (CH Instruments Inc., USA). A charge-coupled device (CCD) camera was also located below the cell to simultaneously monitor pattern formation on the WE surface. For the rotating disk electrode experiments, the working electrode was a 1.1-cm-diameter platinum disk inserted into a Teflon holder, and the

experiment was performed on a rotating disk electrode system (EG&G Model 616). An adjustable resistor was connected in series between the WE and the electrochemical workstation.

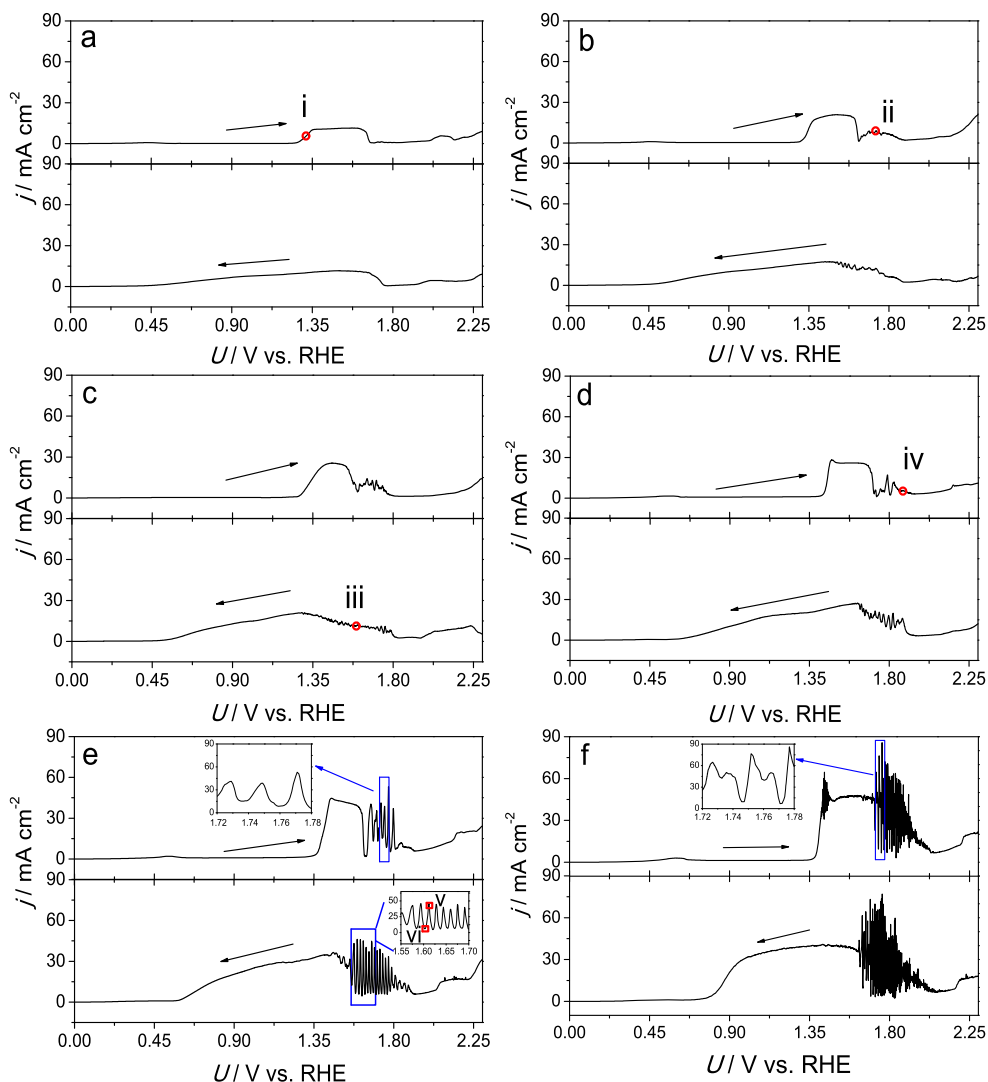
The electrolytes were prepared by dissolving appropriate amounts of analytical reagents such as sodium sulfide and sodium hydroxide (Sinopharm Chemical Reagent Co. Ltd., China) in ultrapure water (Millipore system, 18.2 MΩ cm). Before each experiment was performed, the electrolyte was first degassed by bubbling with pure nitrogen for 20 min, and a nitrogen atmosphere was sustained throughout the entire experiment. The platinum disk was polished to a mirror-like shine using fine alumina powder (0.05 μm) and was then soaked in 0.50 mol L⁻¹ nitric acid for 30 min. After that, the disk was cleaned with ultrapure water in an ultrasonic bath for 5 min. A circulating water bath (Polyscience Instrument, USA) was used to maintain the temperature at 20.0±0.1 °C. A cyclic voltammetry process was then performed between 0.04 and 1.50 V vs. RHE at a scan rate of 50 mV s⁻¹ in 0.50 mol L⁻¹ sulfuric acid for further cleaning of the electrode surface.

Results and discussion

Effect of the sulfide ion concentration

Figure 1 shows the cyclic voltammograms that were recorded during the electro-oxidation of sodium sulfide at various concentrations with a potential scan rate of 0.5 mV s⁻¹. When the sulfide ion concentration was controlled at 0.30 mol L⁻¹, the current density–externally applied potential ($j-U$) curve profile was stable, as shown in Fig. 1a. One large flat peak located at approximately 1.50 V was observed in the positive potential scan, and it was attributed to the electro-oxidation reaction of the sulfide ion when catalyzed by the platinum oxides. Sulfur deposition and dissolution were monitored by the CCD camera and corresponded to the increase and decrease in the current density, respectively. When the sulfide ion concentration was increased to 0.40 mol L⁻¹ in Fig. 1b, the branch with the NDR on both the positive and reverse potential scans of the $j-U$ curve was unstable and began to fluctuate spontaneously. At the same time, self-organized pulses were generated on the electrode surface in the area of current density fluctuation. When the sulfide ion concentration was increased to 0.50 mol L⁻¹ in Fig. 1c, the current density fluctuation became more apparent. This fluctuation gradually changed into larger oscillations with NDR when the sulfide ion concentration increased from 0.60 to 0.80 mol L⁻¹, as shown in Fig. 1d and e. When the sulfide ion concentration increased to 1.00 mol L⁻¹, the dynamic behavior changed abruptly, as shown in Fig. 1f. During the positive potential scan, current density oscillations occurred at approximately 1.45 V on the positive slope area of the $j-U$ curve and were classified as HN-NDR oscillations. The N-NDR oscillations on both the positive and reverse

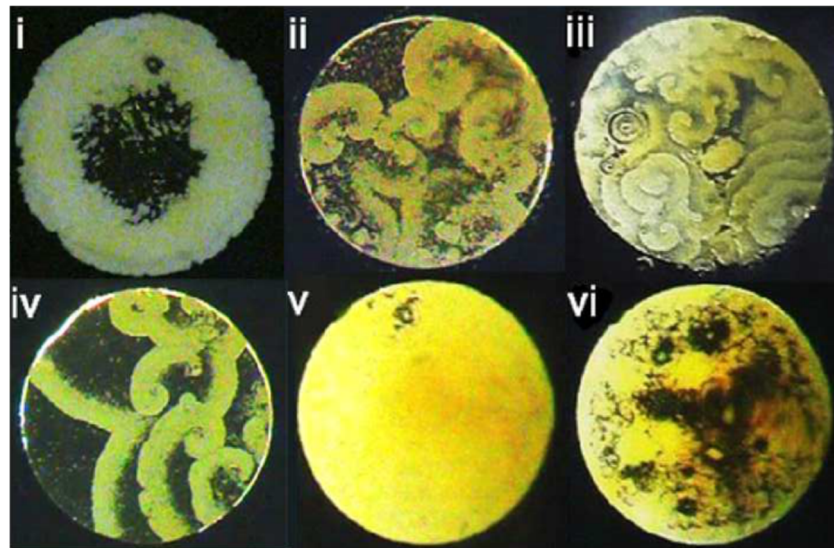
Fig. 1 Cyclic voltammograms of the electro-oxidation of sodium sulfide of various concentrations: **a** 0.30 mol L⁻¹, **b** 0.40 mol L⁻¹, **c** 0.50 mol L⁻¹, **d** 0.60 mol L⁻¹, **e** 0.80 mol L⁻¹, and **f** 1.00 mol L⁻¹; the scan rate was 0.5 mV s⁻¹



potential scans were enhanced in terms of both amplitude and range. The oscillatory period of the N-NDR oscillations also increased with increasing sulfide ion concentration, as shown in the inset curves during the positive potential scans in Fig. 1e and f. Furthermore, the current density was increasing with increasing sulfide ion concentration, from around 10 mA cm^{-2} in Fig. 1a to approximately 75 mA cm^{-2} in Fig. 1f, which indicated that the electro-oxidation reaction of sulfide ions catalyzed by platinum oxides could be promoted by increasing the sulfide ion concentration. As the amplitude and period of the N-NDR oscillations increased with increasing sulfide ion concentration, the synchronous oscillations of sulfur deposition and dissolution became increasingly evident in the N-NDR oscillatory region. The evolution of the pattern formation was simultaneously investigated using the CCD camera. Figure 2 shows the typical self-organized patterns that occurred at the red circles of the cyclic voltammetric curves shown in Fig. 1 during the electro-oxidation of sodium sulfide. In general, the abrupt increases in current density were

related to high levels of sulfur deposition, and it was observed through the CCD camera that the front wave was the main deposition wave, as shown in Fig. 2 (i). With increasing sulfide ion concentration, the current density gradually changed from fluctuation to oscillation. In the N-NDR region, the pulses were monitored within the current density fluctuation region, while synchronous oscillations of sulfur deposition and dissolution were observed in the current density oscillatory area. Fluctuations occurring at the sulfide ion concentration of 0.40 mol L^{-1} corresponded to the pulses shown in Fig. 2 (ii). Spirals were monitored during the reverse potential scan process when the sulfide ion concentration was controlled at 0.50 mol L^{-1} , as shown in Fig. 2 (iii). These spirals were generated at different sites on the disk and could last for a long time, in a similar manner to the famous Belousov–Zhabotinsky (BZ) reaction [25] and were annihilated when they collided with each other or with the edge of the disk (further details are provided in the [Electronic Supplementary Material](#)). In addition, both clockwise and anticlockwise

Fig. 2 Snapshots of the self-organized sulfur deposition patterns that occurred at the *red circles* shown in Fig. 1



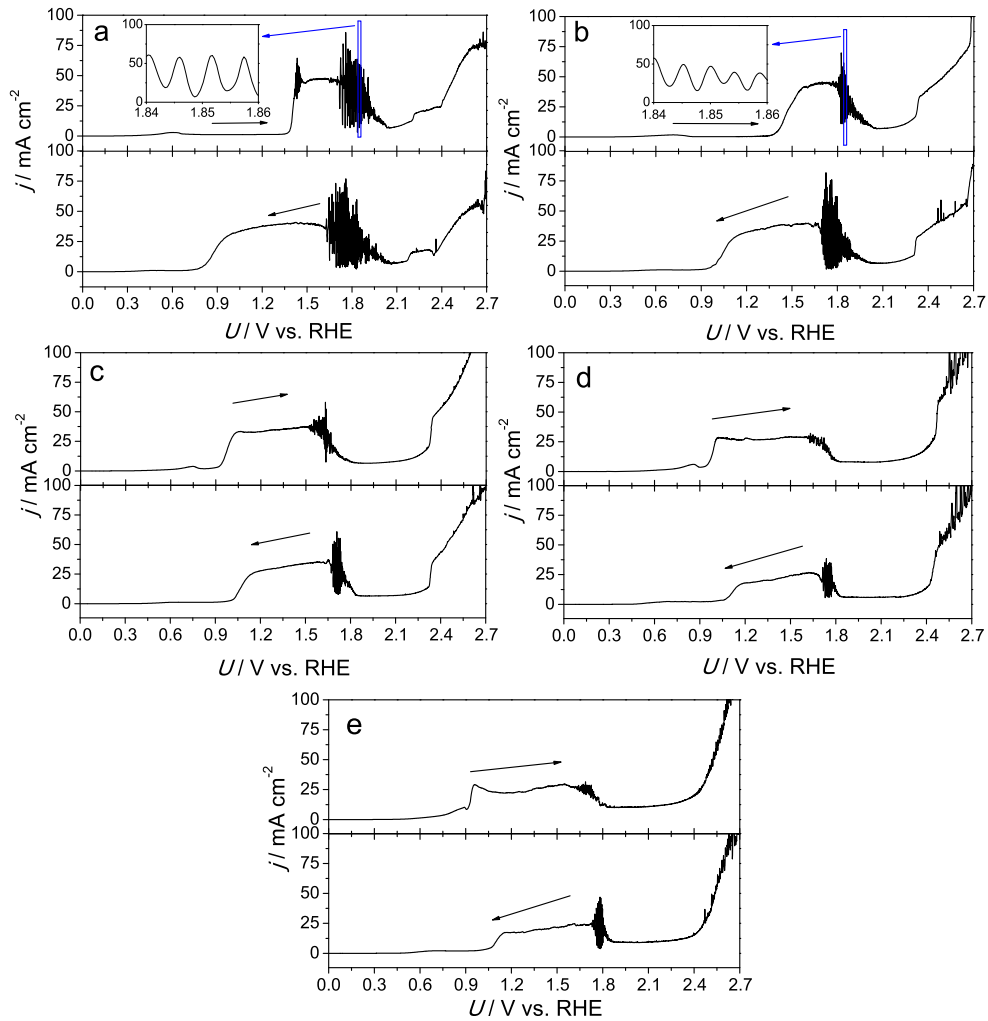
spirals existed in the system, which indicates the coexistence of chirality within the system [26]. With the enhanced fluctuations at the sulfide ion concentration of 0.60 mol L^{-1} , the pulses that were observed through the CCD camera became more obvious, and the pulse width increased when compared with the pulse width at the sulfide ion concentration of 0.40 mol L^{-1} , as shown in Fig. 2 (iv). As the amplitude and period of the N-NDR oscillations increased, the pattern gradually changed into synchronous oscillations of sulfur deposition and dissolution over the entire platinum disk. The discernible synchronous oscillatory phenomenon was observed in Fig. 2 (v and vi). Rising and falling of current densities related to the production and dissolution, respectively, of the sulfur. Continuous oscillations induced repeated deposition and dissolution of sulfur on the platinum surface. In the HN-NDR oscillatory region at the sulfide ion concentration of 1.00 mol L^{-1} in Fig. 1f, slight sulfur deposition and dissolution were observed because of the small oscillatory amplitude with the high current density values. In summary, increases in the sulfide ion concentration resulted in enhancement of both the HN-NDR and N-NDR oscillations. In addition, the patterns in the N-NDR region gradually transformed from local ordered pulses into synchronous oscillations of sulfur deposition and dissolution across the entire disk.

Effects of the hydroxide ion concentration

Because the formation of the platinum oxides gives rise to an N-NDR, which could further develop the positive feedback of electrode potential in the presence of a sufficiently large resistance (including the uncompensated electrolyte resistance and the external resistance), we investigated the influence of the hydroxide ions on the spatiotemporal dynamics in 1.00 mol L^{-1} sodium sulfide electro-oxidation. The results shown in Fig. 3 reveal the effect of the hydroxide ions on

the dynamic behavior during electro-oxidation of 1.00 mol L^{-1} sodium sulfide. In the sodium sulfide solution without initial sodium hydroxide, a white film appeared at approximately 0.60 V in the positive potential scan, which indicated the formation of adsorbed sulfur and thus blocked the active sites of electrode. Consequently, a large potential passivation range was present. However, the passive area was diminished and turned into a higher current density platform with an increase in the hydroxide ion concentration. In addition, both HN-NDR and N-NDR oscillations occurred on the $j-U$ curve without addition of the hydroxide ions, as shown in Fig. 3a. When the 1.00 mol L^{-1} sodium hydroxide was added to the sodium sulfide solution, the HN-NDR oscillations vanished and the amplitude and the potential range of the N-NDR oscillations were reduced, as shown in Fig. 3b. Increasing the initial sodium hydroxide concentration strengthened the inhibition in amplitude and potential range of the oscillations. Only small fluctuations in the current density were observed when the hydroxide ion concentration increased to 3.00 and 4.00 mol L^{-1} , as shown in Fig. 3d and e. Moreover, the onset potential for the abrupt increase in the current density shifted to lower potential values, and the current density platform became gradually wider along the positive potential scan. Comparison of the inset of Fig. 3a with that of Fig. 3b shows that the period and amplitude of the N-NDR oscillations decreased with increasing hydroxide ion concentration. The patterns observed on the electrode surface then consequently changed as shown in Fig. 4a under potentiostatic control. The pulses became obviously irregular and the widths of the pulses gradually decreased with increasing hydroxide ion concentration, which is clearly shown in Fig. 4b. Even more, when the hydroxide ion concentration was increased to more than 2.00 mol L^{-1} , the pulses could barely form on the electrode surface. From the results shown above, we can conclude that both the oscillations and the pattern formation were

Fig. 3 Cyclic voltammograms during electro-oxidation of 1.00 mol L^{-1} sulfides containing various sodium hydroxide concentrations of **a** 0 mol L^{-1} , **b** 1.00 mol L^{-1} , **c** 2.00 mol L^{-1} , **d** 3.00 mol L^{-1} , and **e** 4.00 mol L^{-1} , where the potential is cycled from 0 to 2.7 V at a scan rate of 0.5 mV s^{-1}



restrained by increasing the hydroxide ion concentration during electro-oxidation of the sulfide.

Effect of the external resistance

Figure 5a and b shows cyclic voltammograms of the electro-oxidation of 1.00 mol L^{-1} sodium sulfide with different external resistances at a scan rate of $dU/dt = 0.5 \text{ mV s}^{-1}$. In our previous work [13], we experimentally studied the effects of the external resistance on the oscillatory behavior using the potential sweep method. We found that, when the external resistance was increased from 100 to 150Ω , the N-NDR oscillations were suppressed, and changed into bistable states when the external resistance was increased to 275Ω . Three HN-NDR oscillatory regions (one in the low potential region and two in the high potential ranges) were observed in the cyclic voltammograms with increasing external resistance. Here, we concentrated on the spatiotemporal dynamics under potentiostatic conditions. The amplitude and the potential range of the HN-NDR oscillations increased with increasing resistance, while the N-NDR oscillatory behavior was

suppressed, as shown in Fig. 5a and b. The potentiostatic experiments were performed to study the N-NDR oscillations as part of a wider investigation of the spatiotemporal dynamics of the system. Time series of the current density oscillations with the external resistance of 100Ω are shown in Fig. 5c to f for various external potentials. When the potential was fixed at 1.70 V , the current density oscillated in a simple mode, as shown in Fig. 5c. The current density then experienced an abrupt increase to approximately 83 mA cm^{-2} . This sudden increase in current density was accompanied by the rapid deposition of sulfur across the entire WE surface, as observed by the CCD camera. The deposited sulfur reacts with the bulk sulfide to generate yellow polysulfide ions that slowly dissolve into the solution [27]. The current density then decreased gradually to a plateau at approximately 44 mA cm^{-2} . Immediately after that plateau, there was a sharp reduction in the current density to almost 0 mA cm^{-2} . After a short time, the current density rose again, and a similar pattern formation and evolution were observed. The synchronous oscillations of the sulfur deposition and dissolution thus occurred repeatedly with the current oscillations over the entire WE surface. When the

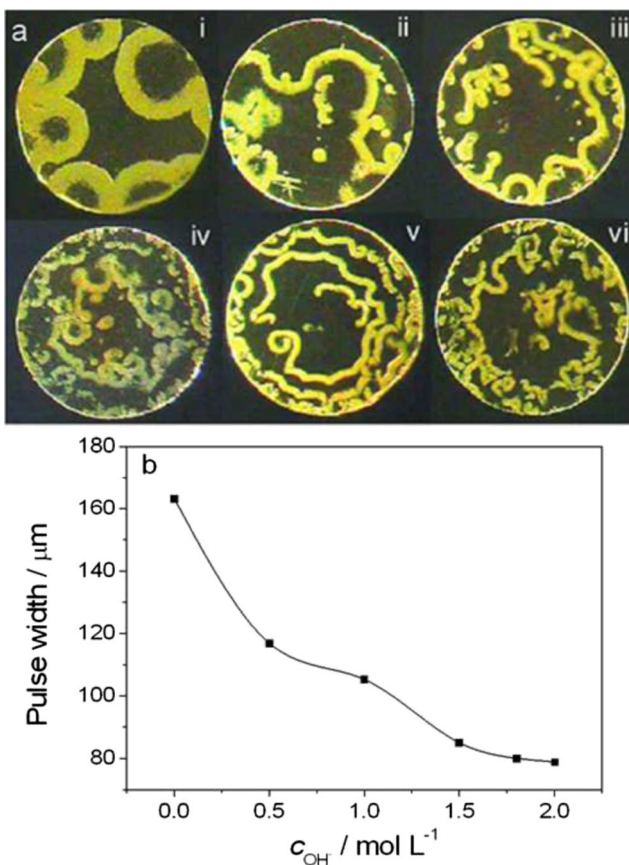


Fig. 4 **a** Morphology and **b** width of the pulses in the electro-oxidation of 1.00 mol L^{-1} sodium sulfide under conditions of: (i) $[\text{OH}^-]_0 = 0 \text{ mol L}^{-1}$, 1.96 V ; (ii) $[\text{OH}^-]_0 = 0.50 \text{ mol L}^{-1}$, 1.84 V ; (iii) $[\text{OH}^-]_0 = 1.00 \text{ mol L}^{-1}$, 1.72 V ; (iv) $[\text{OH}^-]_0 = 1.50 \text{ mol L}^{-1}$, 1.62 V ; (v) $[\text{OH}^-]_0 = 1.80 \text{ mol L}^{-1}$, 1.62 V ; and (vi) $[\text{OH}^-]_0 = 2.00 \text{ mol L}^{-1}$, 1.60 V

potential was increased to 1.85 V , the current density also oscillated spontaneously with time, as shown in Fig. 5d. However, the time duration of the high current density plateau decreased. Along the ascending section of the current density, small oscillations were observed, and these oscillations were more obvious at the potential of 1.95 V in Fig. 5e. Complex oscillations are shown in Fig. 5e with more prolonged small oscillations and a shorter high current density plateau. The CCD camera detected a novel pattern on the WE surface that was composed of local pulses at the small oscillation stage and synchronous oscillations of sulfur deposition and dissolution during the abrupt increases and decreases in the current density, i.e., alternating behavior between local patterns and synchronous oscillations of sulfur deposition and dissolution was observed on the WE surface, as shown in Fig. 6a. Further increases in the potential induced gradual damping of the oscillations, and when the potential was maintained at 2.20 V , the oscillations were transformed into a stable state with very low current density, as shown in Fig. 5f. At this point, no deposition pattern was found on the WE surface.

As discussed above, when the external resistance of 100Ω was in series with the circuit, the sulfide electro-oxidation

system experienced complex current density oscillations composed of small and large oscillations. Meanwhile, the patterns that formed on the electrode surface were alternating synchronous oscillations of sulfur deposition and dissolution and local pulses, as shown in Fig. 6. In the small oscillatory region, the deposition pulses were stimulated from the edge of the electrode disk and propagated toward the center (inset i in Fig. 6a). Then, an abrupt increase in the current density induced sudden deposition of sulfur over the entire electrode surface (inset ii in Fig. 6a). After that, the current density decreased slowly before dropping straight away to almost zero, and as a result, nearly bare platinum was observed (inset iii in Fig. 6a). The local pulses and the synchronous oscillations of sulfur deposition and dissolution occurred repeatedly, forming the alternating patterns. This behavior can be clearly distinguished in the space-time diagram (Fig. 6b) for the red line crossing the disk center, as shown in Fig. 6a. Figure 6b only shows the pattern in one-dimensional space, and the evolution of the alternating patterns in two-dimensional space is shown in more detail in a movie in the [Electronic Supplementary Material](#).

Mechanism analysis and discussion

The electro-oxidation of sodium sulfide on platinum is found to exhibit rich and complex spatiotemporal dynamic behavior. Both HN-NDR and N-NDR oscillations and abundant patterns are observed in this simple system. In addition, the oscillatory amplitude, period, and potential range can be controlled by simply adjusting the species concentrations and the external resistance. As discussed in the literature [13, 22, 24], the following reactions were expected to take place at the electrode/electrolyte interface in the sulfide system, thus resulting in the observed complex spatiotemporal dynamics:

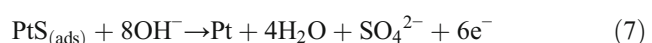
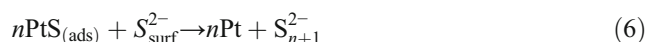
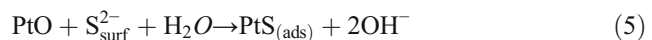
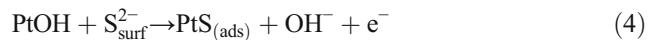
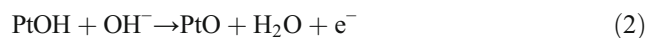
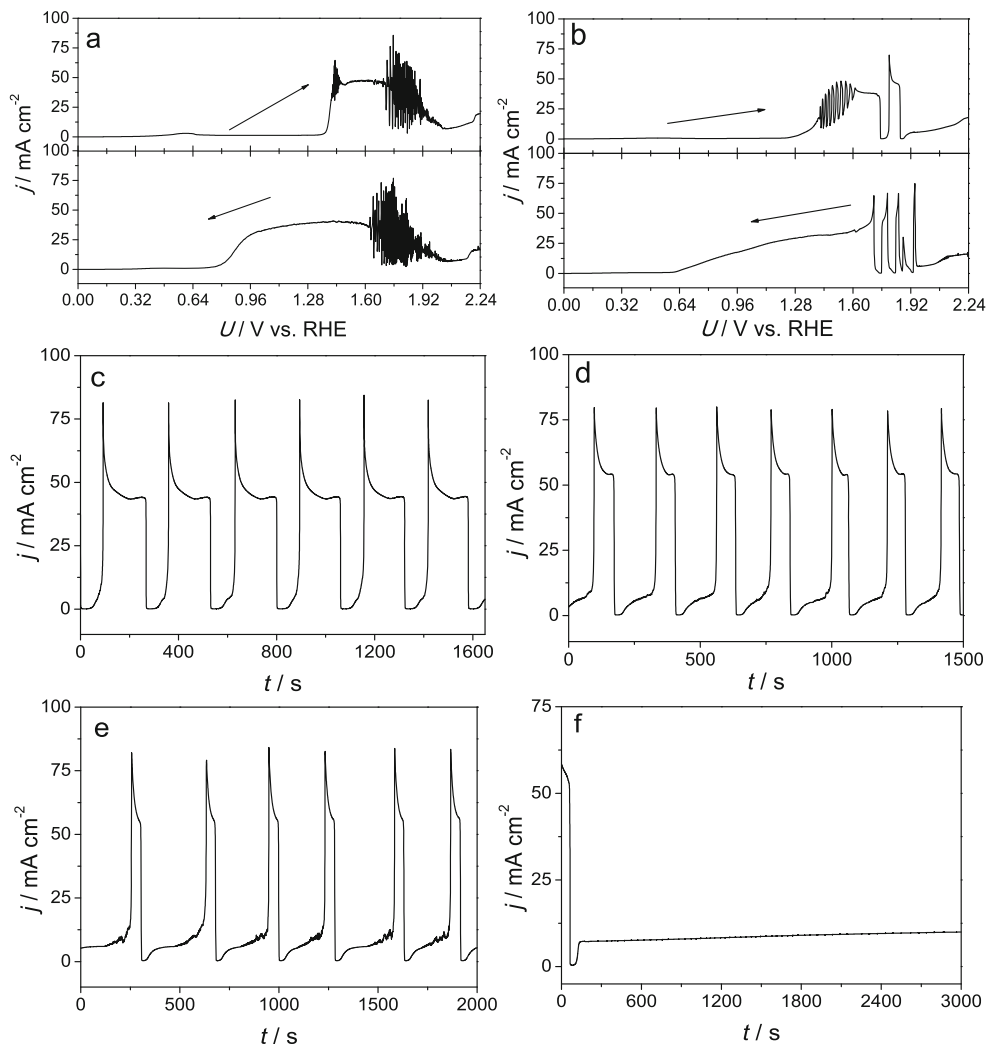


Fig. 5 Effect of the external resistance on the oscillatory dynamics. Cyclic voltammograms with **a** 0 Ω and **b** 100 Ω external resistances at a potential scan rate of 0.5 mV s $^{-1}$, time series of current density under potentiostatic control at **c** 1.70 V, **d** 1.85 V, **e** 1.95 V, and **f** 2.20 V with external resistance of 100 Ω



Here, the subscripts bulk, surf, and ads denote bulk solution, electrode surface, and adsorbed surface species, respectively, and n is a positive integer. The formation of the platinum oxides (reactions 1 and 2) gives rise to the NDR in this

system. The platinum oxides can catalyze the oxidation of the surface sulfide ion, which is supplemented through the mass-transfer process (reaction 3) to generate elemental sulfur (reactions 4 and 5). The deposited sulfur reacts directly with

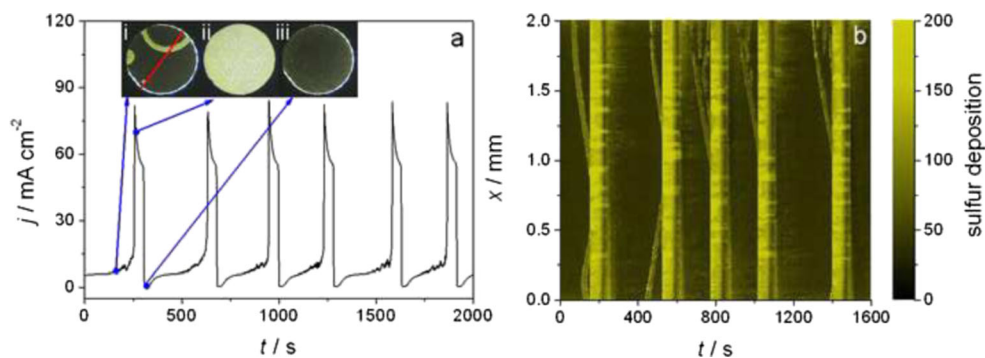


Fig. 6 Spatiotemporal dynamics during potentiostatic control at 1.95 V with an external resistance of 100 Ω . **a** Evolution of both the current density and the alternating patterns between local pulses and synchrony.

b Space–time diagram at the red line in **a** of the alternating patterns, where the yellow areas represent deposited sulfur and the dark areas represent bare platinum

the surface sulfide ion to produce soluble polysulfide ions through reaction 6, which as a result regenerates the active sites of the platinum electrode to repeat the above electrochemical reactions. The deposited sulfur can also be oxidized directly into sulfate through reaction 7 at high potentials. Thus, in the HN-NDR oscillatory region, reactions 1 and 2 induce the formation of the platinum oxides and act as the positive feedback. However, the surface sulfide ion concentration is high, and the active sites can be occupied rapidly through reactions 4 and 5, and, as a result, inhibit the formation of the platinum oxides. Following reactions 4 and 5, the surface-deposited sulfur is dissolved through reaction 6. In addition, the direct oxidation of the deposited sulfur into the sulfate (reaction 7) also occurs. Reactions 6 and 7 are both potential-dependent reactions. Therefore, the consecutive processes of reactions 4 and 5 are treated as the negative feedback because they inhibit the formation of the platinum oxides.

For the N-NDR oscillations, the positive feedback is also composed of reactions 1 and 2. After the heavy consumption of the surface sulfide ions in the increasing current density region, the supplementation of the surface sulfide ions (reaction 3) is the slow but key step that limits the reproduction of the deposited sulfur (reactions 4 and 5) and the unoccupied platinum sites (reactions 6 and 7). Thus, the mass-transfer limited process (reaction 3) is the negative feedback in this case, which can be demonstrated by the rotating disk electrode results shown in Fig. 7. When the disk is rotating, reaction 3 is accelerated, which means that the damage of the negative feedback results in the suppression of the N-NDR oscillations. In summary, HN-NDR and N-NDR oscillations have the same positive feedback of the electrode potential, but different negative feedbacks (i.e., competitive adsorption of the deposited sulfur for the HN-NDR oscillations and the mass-transfer limited process for the N-NDR oscillations). Figure 8 provides a conclusive summary that illustrates the two oscillatory mechanisms. For the HN-NDR oscillations, the oscillatory loop starts with the formation of the platinum oxides (reactions 1 and 2), followed by the adsorption of the deposited sulfur (reactions 4 and 5), and the renewal of the platinum active sites to repeat the loop. The adsorption of the deposited sulfur (reactions 4 and 5) can inhibit the formation of the platinum

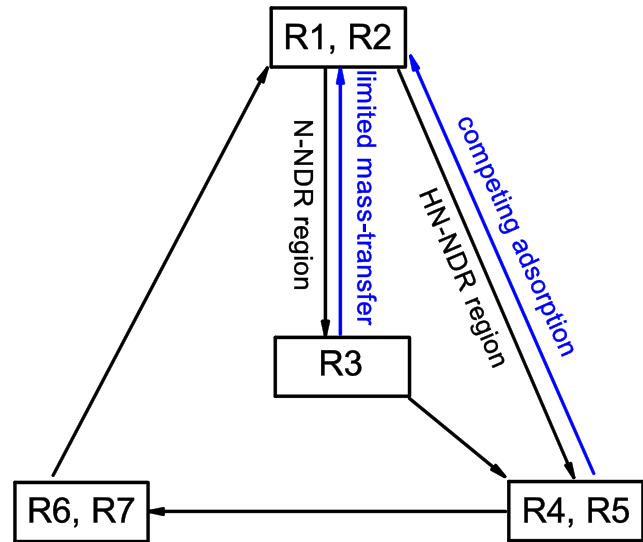


Fig. 8 Oscillatory loops of the electro-oxidation of sulfide in the HN-NDR and N-NDR regions

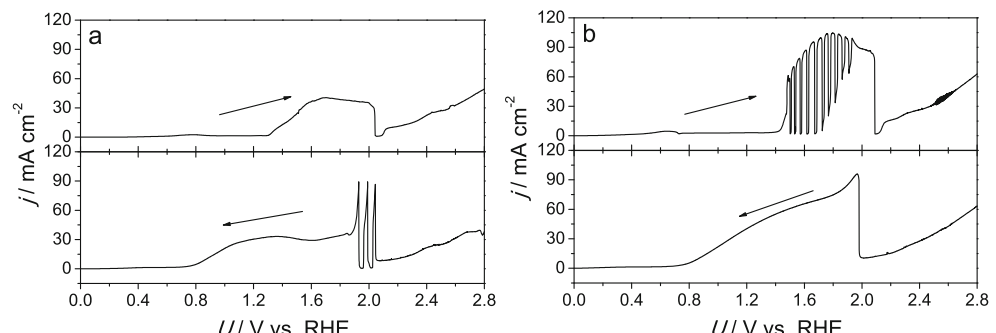
oxides, and thus reactions 4 and 5 act as the negative feedbacks in the HN-NDR oscillatory region. For the N-NDR oscillations, the oscillatory loop also starts with reactions 1 and 2. However, after the abrupt consumption of the sulfide ions in the HN-NDR region, the mass-transfer process (reaction 3) then limits the formation of the platinum oxides. Thus, reaction 3 is the negative feedback in the N-NDR oscillatory region.

Based on the mechanisms described here, and considering the charge balance of the circuit, the mass balance and the potential dependence of the sulfur adsorption, we build a dimensionless model to explain the dynamic behavior of the sulfide system. The detailed derivation of the model is presented in the [Electronic Supplementary Material](#). The model contains:

$$\frac{d\phi}{dt} = \frac{u-\phi}{r} - m_p c(1-\theta)k(\phi) \quad (8)$$

$$\frac{dc}{dt} = 1-c + \beta c \frac{u-\phi}{r} - c(1-\theta)k(\phi) - k_2 c \theta \quad (9)$$

Fig. 7 Cyclic voltammograms in 0.50 mol L⁻¹ sodium sulfide with rotation rates of **a** 0 rpm and **b** 100 rpm, where the scan rate was 0.5 mV s⁻¹



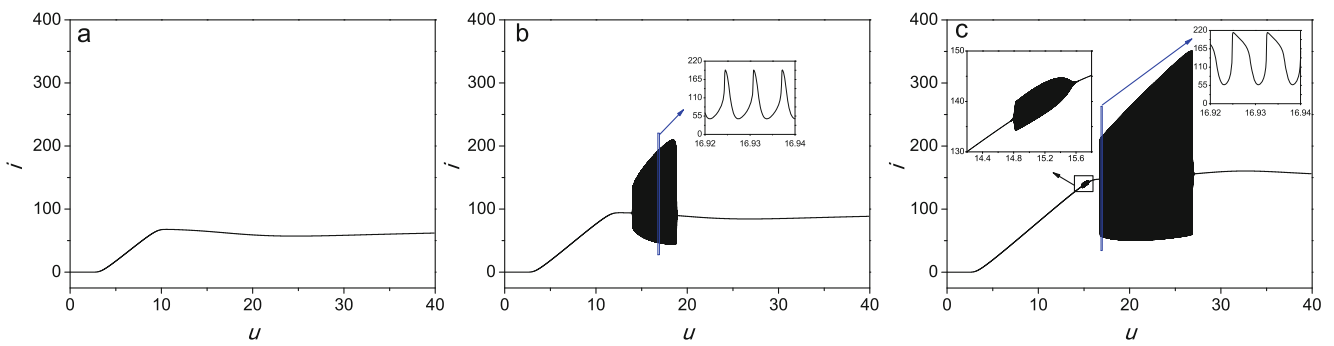


Fig. 9 Simulated linear sweep voltammograms for various sulfide ion concentrations at **a** $m_p=2600$, **b** $m_p=3600$, and **c** $m_p=5600$. The parameter values are $r=0.077$, $\beta=0.1$, $x_p=0.0001$, $P=1.2$, $k_2=2.0$, $k_0=38$, $e_d=3.98$, $b=9.2$, $M=3.0$, and $du/dt=0.001$

$$\frac{d\theta}{dt} = P \left[\frac{1}{1 + e^{(\phi-4.7)/0.2}} - \theta \right] \quad (10)$$

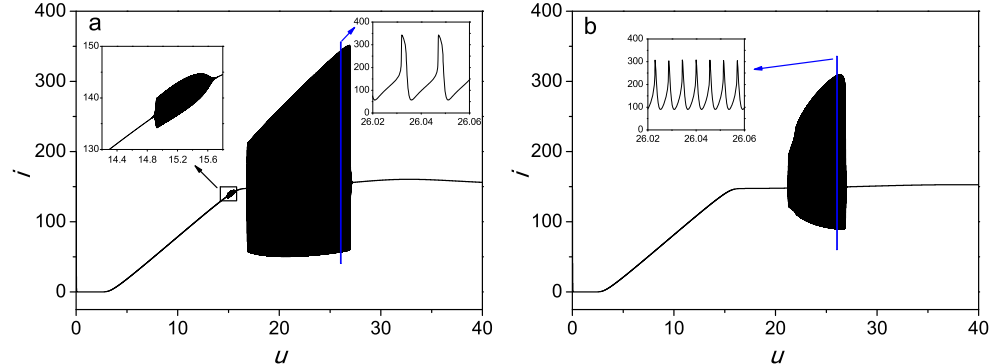
with

$u = \frac{nF}{RT} U$, $m_p = \frac{n^2 F^2 c_{\text{bulk}}}{CRT}$, $\beta = \frac{2\mu RT A C R_s}{nF\delta l}$, $r = \frac{2D A C R_s}{\delta^2}$, $k_2 = \frac{\delta^2 k_1}{2D}$ and $k(\phi) = k_0 \left(x_p \phi^2 + \frac{b}{M + (\phi - e_d)} \right)^2$, where ϕ , c , and θ stand for the dimensionless variables for double-layer potential, interface concentration of sulfide ion, and sulfur coverage on the electrode surface, respectively, and the two parameters, u and r , are the dimensionless external potential and the dimensionless resistance, respectively. The meanings of the other parameters are given in the [Electronic Supplementary Material](#). In this model, the subsystems of (8)+(9) and (8)+(9) represent the N-NDR and HN-NDR dynamics, respectively. The three-variable model comprising Eqs. 8, 9, and 10 can be used to simulate the sulfide electro-oxidation system. The effects of the various factors on the spatiotemporal dynamics can thus be clearly analyzed. The dimensionless total electric current is calculated from the formula $i=(u-\phi)/r$.

In the model simulation, an increase in the bulk sulfide ion concentration causes an equivalent increase in the parameter m_p because it contains the bulk sulfide ion concentration. The simulated results show that HN-NDR and N-NDR oscillations are both promoted by

increasing m_p , as shown in Fig. 9, which is consistent with the experimental results shown in Fig. 1. In the positive slope region of current, the surface sulfide concentration is high. When the bulk sulfide ion concentration increases, the renewal of the active platinum sites (reaction 6) is accelerated and, as a result, enhances the positive feedback for the generation of the platinum oxides (reactions 1 and 2). The HN-NDR oscillations are thus induced by the increasing sulfide ion concentration. In the negative slope region of current, the surface sulfide ion concentration is low because of the heavy consumption in the positive slope region of current, which limits the deposition reactions (reactions 4 and 5). Increasing the initial bulk sulfide ion concentration thus induces an increase in the surface sulfide ion concentration to generate greater sulfur coverage on the electrode surface. As a result, the formation of the platinum oxides is restrained, which slows down the positive feedback and causes an increase in the oscillatory period. However, the external potential range for the N-NDR oscillations is extended because the deceleration of the positive feedback is beneficial to the oscillations along the negative slope region of current when the initial bulk sulfide ion concentration is increasing. Considering the spatial coupling, the increase in the

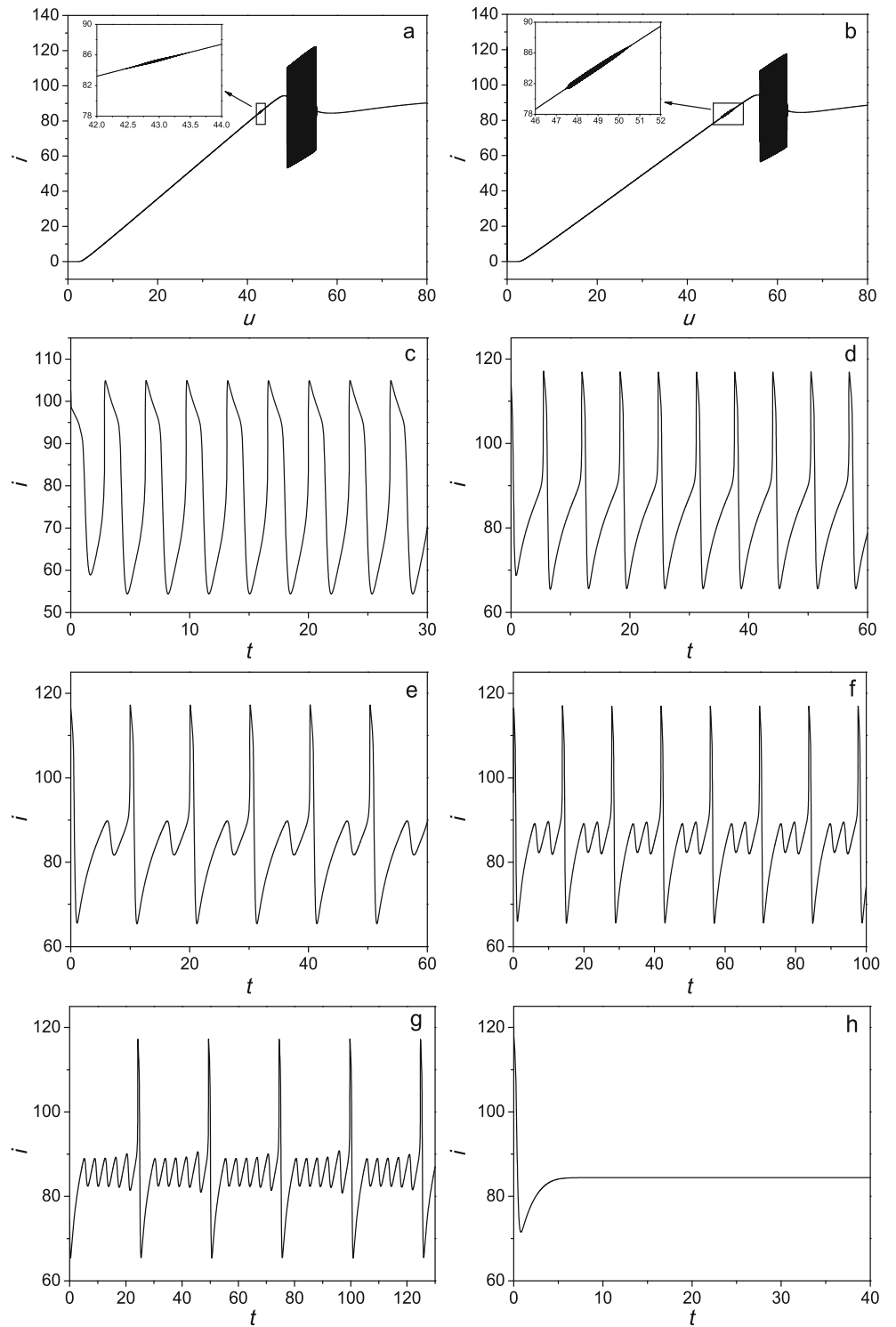
Fig. 10 Simulated linear sweep voltammograms for various hydroxide ion concentrations at **a** $b=9.2$ and **b** $b=30$. The parameter values are $r=0.077$, $\beta=0.1$, $x_p=0.0001$, $P=1.2$, $k_2=2.0$, $k_0=38$, $e_d=3.98$, $M=3.0$, $m_p=5600$, and $du/dt=0.001$



oscillatory amplitude and period results in the pattern transition from pulses to synchronous oscillations of sulfur deposition and dissolution in the region of the N-NDR oscillations when the initial bulk sulfide ion concentration is increased, which can explain the experimental results shown in Fig. 2.

Fig. 11 Simulated results of the external resistance effect on the oscillatory dynamics. Linear sweep voltammograms with increasing resistance **a** $r=0.454$ and **b** $r=0.531$ are shown, along with time series of the total currents under potentiostatic control at **c** $u=54.4$, **d** $u=62.13$, **e** $u=62.14$, **f** $u=62.148$, **g** $u=62.15$, and **h** $u=64.50$ with $r=0.531$. The parameter values are $\beta=0.1$, $x_p=0.0001$, $P=1.2$, $k_2=2.0$, $k_0=38$, $e_d=3.98$, $b=9.2$, $m_p=3600$, $M=3.0$, and $du/dt=0.001$

In the model, the parameter b in $k(\phi)$ is related to the hydroxide ion concentration. When ϕ is driven towards large values, the larger value of b causes a greater reduction in the Faradaic current, which can be beneficial for the positive feedback of the electrode potential ϕ . In the experiments as shown in Figs. 3 and 4, increasing the hydroxide ion concentration



induced suppression of both the HN-NDR and N-NDR oscillations in terms of amplitude and potential range as well as the period, and the local pulses are reduced in width. In the model simulation, an increase in the parameter b produced the same discipline that is shown in Fig. 10. As the hydroxide ion concentration increases, the formation of the platinum oxides (reactions 1 and 2) is accelerated, leading to a reduction in the oscillatory period. When the rates of reactions 1 and 2 far exceed that of reactions 4 and 5, the oscillations would be restrained. The HN-NDR oscillations change to a stable state when b increases from 9.2 to 30, while the N-NDR oscillations are reduced in both amplitude and range. The reduced pulse widths (Fig. 4) with increasing hydroxide ion concentration are a result of the reduction of the oscillatory period according to the relationship between the pattern wavelength and the dynamic period in the reaction–transportation system.

In general HN-NDR and N-NDR electrochemical oscillators, the resistance (including both the uncompensated electrolyte resistance and the external resistance) has a crucial effect on the dynamic behavior. For the HN-NDR system, the oscillations are extended with increasing resistance; while in the N-NDR system, the oscillatory behavior changes into a bistable state when the resistance exceeds a certain critical value [8, 9, 19]. Here, with the model simulation, we derive the same result as that shown in Fig. 11. In the potential scan mode, increasing the resistance, r , from 0.454 to 0.531 causes the N-NDR oscillatory range to decrease from $\Delta u=6.72$ to 6.33. However, the HN-NDR oscillations are apparently enhanced in the external potential range and amplitude shown in the inset curves in Fig. 11a and b. When the resistance is fixed at 0.531, an increase in the external potential in the N-NDR oscillatory region causes a change in the oscillatory behavior from simple oscillations to complex oscillations before a stable state is reached. Through the interplay between the local dynamics and the spatial coupling, the small and large peaks of the complex oscillations produce the pulses and the synchronous oscillations of sulfur deposition and dissolution, respectively, which causes the novel pattern formation in the experiments of alternating local pulses and synchronous oscillations of sulfur deposition and dissolution.

Conclusions

The effects of both the sulfide and hydroxide ion concentrations and the external resistance on the spatiotemporal dynamics during the electro-oxidation of sodium sulfide were investigated on a platinum disk with simultaneous CCD camera observation. In this electrochemical system, the formation of the platinum oxides gives rise to an NDR, resulting in the positive feedback of the electrode potential. The adsorption of elemental sulfur and the mass transportation-limited

processes of the sulfide ion act as negative feedbacks for the HN-NDR and N-NDR oscillations, respectively. Increasing the sulfide ion concentration benefits both the HN-NDR and N-NDR oscillations. The self-organized pattern that formed in the NDR region started with a sulfur deposition front wave and gradually changed from pulses to synchronous oscillations of sulfur deposition and dissolution through increases in the initial bulk sulfide ion concentration. Increasing the hydroxide ion concentration can promote the formation of the platinum oxides and the positive feedback is strengthened, resulting in reduction of the oscillatory period, the amplitude, and the pulse width. The external resistance was another factor that resulted in enhancement of the HN-NDR oscillations and inhibition of the N-NDR oscillations. In addition, a novel pattern formation of alternating local pulses and synchronous oscillations of sulfur deposition and dissolution can be observed. A designed three-variable model of this mechanism can numerically analyze the HN-NDR and N-NDR oscillations and also qualitatively explained the spatiotemporal pattern. In addition, we are currently working on the interplay between the homogeneous dynamics and the spatial coupling, and a systematic analysis based on the pattern simulation will be published in the future. In summary, we believe that this investigation will further promote the study of complex spatiotemporal dynamic processes and will also be helpful in the prediction and control of pattern formation. The sulfide electro-oxidation system could become a well-known system similar to the BZ reaction and has encouraging future prospects.

Acknowledgments This work was supported in part by a grant (No. 51221462) from the National Natural Science Foundation of China, a grant (No. BK20131111) from JSNSF, the Fundamental Research Funds for the Central Universities, China (No. 2013XK05), the Priority Academic Program Development of Jiangsu Higher Education Institutions, and the Program for Graduate Research and Innovation in Universities of Jiangsu Province, China (No. CXLX13-947).

References

- Lev O, Sheintuch M, Pisemen LM, Yarnitzky C (1988) Standing and propagating wave oscillations in the anodic dissolution of nickel. *Nature* 336:458–459
- Sazou D, Pavlidou M, Diamantopoulou A, Pagitsas M (2012) Oscillatory phenomena as a probe to study pitting corrosion of iron in halide-containing sulfuric acid solutions. In: Bensalah N (ed) Pitting corrosion. In Tech, Rijeka, pp 61–92
- Nagamine Y, Yoshikawa K (2010) Contribution of convection to spatiotemporal stripe patterns formed by Ag and Sb coelectrodeposition. *Chaos* 20:023117-1–023117-11
- Krastev I, Dobrovolska T (2013) Pattern formation during electrodeposition of alloys. *J Solid State Electrochem* 17:481–488
- Lopes PP, Ticianelli EA, Varela H (2011) Potential oscillations in a proton exchange membrane fuel cell with a Pd–Pt/C anode. *J Power Sources* 196:84–89

6. Wickramasinghe M, Kiss IZ (2013) Spatially organized dynamical states in chemical oscillator networks: synchronization, dynamical differentiation, and chimera patterns. *PLoS One* 8:e80586
7. Koper MTM (1992) The theory of electrochemical instabilities. *Electrochim Acta* 37(10):1771–1778
8. Krischer K (2003) Nonlinear dynamics in electrochemical system. In: Alkire RC and Kolb DM (eds) *Advances in electrochemical science and engineering*, Vol. 8. Wiley-VCH, Weinheim, pp 89–208
9. Orlik M (2012) Self-organization in electrochemical systems. I: general principles of self-organization. *Temporal instabilities*. Springer, Berlin Heidelberg New York
10. Orlik M (2012) Self-organization in electrochemical systems. II: spatiotemporal patterns and control of chaos. Springer, Berlin Heidelberg New York
11. Ijzermans AB (1969) Poisoning effects of hydrogen sulfide on noble metal electrodes. Part II: effect of H₂S on periodic current vs. potential curves of Pt and Au electrodes in 0.5 M H₂SO₄. *Recueil des Travaux Chimiques des Pays-Bas* 88:344–352
12. Batista BC, Ferreira GCA, Varela H (2011) The effect of poisoning species on the oscillatory dynamics of an electrochemical reaction. *J Phys Conf Ser* 285:012003-1–012003-8
13. Zhao Y, Wang S, Varela H, Gao Q, Hu X, Yang J, Epstein IR (2011) Spatiotemporal pattern formation in the oscillatory electro-oxidation of sulfide on a platinum disk. *J Phys Chem C* 115:12965–12971
14. Birzu A, Plenge F, Jaeger NI, Hudson JL, Krischer K (2003) Complex spatiotemporal antiphase oscillations during electrodissolution of a metal disk electrode: model calculations. *J Phys Chem B* 107:5825–5835
15. Birzu A, Plenge F, Jaeger NI, Hudson JL, Krischer K (2003) Excitable dynamics during electrodissolution of a metal disk electrode: model calculations. *Phys Chem Chem Phys* 5:3724–3731
16. Krischer K, Varela H, Birzu A, Plenge F, Bonnefont A (2003) Stability of uniform electrode states in the presence of ohmic drop compensation. *Electrochim Acta* 49:103–115
17. Plenge F, Varela H, Krischer K (2005) Pattern formation in stiff oscillatory media with nonlocal coupling: a numerical study of the hydrogen oxidation reaction on Pt electrodes in the presence of poisons. *Phys Rev E* 72:066211-1–066211-11
18. Mazouz N, Flatgen G, Krischer K (1997) Tuning the range of spatial coupling in electrochemical systems: from local via nonlocal to global coupling. *Phys Rev E* 55:2260–2266
19. Kiss IZ, Nagy T, Gáspár V (2011) Dynamical instabilities in electrochemical processes. In: Kharton VV (ed) *Solid state electrochemistry. II: electrodes, interfaces and ceramic membranes*, 1st edn. Wiley-VCH Verlag GmbH & Co. KgaA, Weinheim, pp 125–178
20. Schmidt L, Schönleber K, Krischer K, García-Morales V (2014) Coexistence of synchrony and incoherence in oscillatory media under nonlinear global coupling. *Chaos* 24:013102-1–013102-7
21. Helms H, Schrömer E, Jansen W (1998) Oscillation phenomena during the electrolysis of alkaline sulfide solutions on platinum electrodes. *Monatsh Chem* 129:617–623
22. Feng J, Gao Q, Xu L, Wang J (2005) Nonlinear phenomena in the electrochemical oxidation of sulfide. *Electrochim Commun* 7: 1471–1476
23. Miller B, Chen A (2006) Oscillatory instabilities during the electrochemical oxidation of sulfide on a Pt electrode. *J Electroanal Chem* 588:314–323
24. Yang JP, Song YA, Varela H, Epstein IR, Bi WY, Yu HY, Zhao YM, Gao QY (2013) The effect of chloride on spatiotemporal dynamics in the electro-oxidation of sulfide on platinum. *Electrochim Acta* 98: 116–122
25. Vanag VK, Epstein IR (2001) Inwardly rotating spiral waves in a reaction-diffusion system. *Science* 294:835–837
26. Ernst KH (2013) Molecular chirality in surface science. *Surf Sci* 613:1–5
27. Szynkarczuk J, Komorowski PG, Donini JC (1995) Redox reactions of hydrosulphide ions on the platinum electrode. II: an impedance spectroscopy study and identification of the polysulphide intermediates. *Electrochim Acta* 40:487–494